

https://doi.org/10.26650/ijegeo.1647738

Submitted: 26.02.2025 Revision Requested: 24.03.2025

Last Revision Received: 25.03.2025

Accepted: 21.05.2025

# **International Journal of Environment and Geoinformatics**

Research Article 6 Open Access

# Optimization of Thermal Processing for Enhancing Superconducting Phase Fractions in Ternary Fullerides via a Drop-Quenching Approach



H. Esma Okur 1 D

#### Abstract

This study explores an optimized thermal protocol for synthesizing ternary superconducting fullerides, focusing on enhancing the face-centered-cubic (fcc) phase fraction while mitigating the formation of competing thermodynamically stable phases. Unlike previous studies, which primarily investigated annealing conditions, this work introduces a drop-quenching approach—rapid cooling in ice/water baths (-3°C to 1°C)—as a potential means to influence phase formation. The expanded ternary fulleride, K<sub>0.3</sub>Cs<sub>2.7</sub>C<sub>6.0</sub>, was synthesized through a precursor-based solid-state synthetic route. The impact of two annealing temperatures (430°C and 480°C) and two cooling methods (drop-quenching vs. ambient air cooling) was systematically examined. X-ray powder diffraction confirms that K<sub>0.3</sub>Cs<sub>0.7</sub>C<sub>60</sub> adopts a cubic structure with fcc symmetry. Magnetization measurements reveal that the material exhibits superconductivity with a critical temperature  $(T_c)$  of 29.9 K. Structural characterizations shows that increasing the annealing temperature from 430°C to 480°C, combined with intermittent regrinding and pelletization, improved fcc-phase fractions and lattice expansion. However, the difference between quench cooling and natural cooling in air is found to be minimal. These findings suggest that increasing the annealing temperature to 480°C could be beneficial for the synthesis of expanded ternary fullerides by enhancing the superconducting fcc-phase fractions and addressing challenges posed by the increased size mismatch of the substituted cations relative to the interstitial sites in the fcc structure.

#### **Keywords**

A<sub>3</sub>C<sub>60</sub> · Ternary Fullerides · Superconductivity · Drop-quench · Thermal Optimization



- Citation: Okur, H. E. (2025). Optimization of thermal processing for enhancing superconducting phase fractions in ternary fullerides via a drop-quenching approach. *International Journal of Environment and Geoinformatics*, 12(3), 227-234. https://doi.org/10.26650/ijegeo.1647738
- 😊 This work is licensed under Creative Commons Attribution-NonCommercial 4.0 International License. 🛈 🗞
- © 2025. Okur, H. E.
- ☑ Corresponding author: H. Esma Okur esma.okur@btu.edu.tr



<sup>&</sup>lt;sup>1</sup> Bursa Technical University, Faculty of Engineering and Natural Sciences, Department of Chemistry, Bursa, Türkiye

## Introduction

Superconducting A<sub>3</sub>C<sub>60</sub> compounds, where A represents alkali metals, have garnered significant interest due to their similarities with unconventional superconductors like cuprates, iron pnictides, and heavy fermions. These similarities include the emergence of superconductivity from an antiferromagnetic Mott insulating state under physical or chemical pressure and a dome-shaped critical temperature dependence, highlighting the role of strong electron correlations (Lee et al., 2006; Si & Steglich, 2010; Uemura, 2009). The superconducting pairing mechanism in fullerides is widely accepted to involve strong electron correlations, electron-phonon interactions, and molecular Jahn-Teller (JT) distortions (Alloul et al., 2017; Ganin et al., 2008, 2010; Ihara et al., 2010, 2011; Kasahara et al., 2014, 2017; Klupp et al., 2012; Menelaou et al., 2018; Nomura et al., 2015; Potocnik et al., 2014; Potočnik et al., 2014; Takabayashi et al., 2009; Takabayashi & Prassides, 2016b, 2016a; Wzietek et al., 2014; Zadik et al., 2015, 2018).

Studies consistently show that transitions between electronic ground states in A<sub>3</sub>C<sub>60</sub> fullerides are primarily governed by changes in interfullerene spacing, which in turn modulate the electronic bandwidth (W). This modulation can be induced by two distinct means: physical pressure, applied externally via hydrostatic compression, and chemical pressure, introduced internally through substitution of the alkali cations with smaller ones. In the archetypal Mott-Jahn-Teller insulator (MJTI) Cs<sub>3</sub>C<sub>60</sub>, applying physical pressure reduces the unit cell volume, thereby increasing W and driving a transition to a metallic, and ultimately superconducting state (Ganin et al., 2008, 2010). Similarly, chemical pressure—achieved by substituting the larger Cs<sup>+</sup> ions with smaller Rb<sup>+</sup> or K<sup>+</sup> ions leads to lattice contraction and comparable changes in the electronic structure. The insulating MJTI state first evolves into a Jahn-Teller metallic (JTM) state, where localized JT-active electrons coexist with itinerant ones. Upon further cooling, the localized behavior gradually fades, giving rise to a metallic state that retains cubic symmetry. At even lower temperatures, superconductivity emerges, with the critical temperature  $(T_c)$ exhibiting a dome-shaped dependence on the molecular volume (V) occupied by each  $C_{60}^{3-}$  anion (Zadik et al., 2015).

Application of chemical pressure to fcc  $Cs_3C_{60}$  to increase W is achieved by manipulating both the type and quantity of metals occupying the fcc tetrahedral interstitial cavities ( $T_d$ , two per  $C_{60}$  unit with a radius of 1.12 Å), rather than the octahedral ones ( $O_h$ , one per  $C_{60}$  unit with a radius of 2.06 Å). Because the  $T_d$  cavities are smaller compared to the  $O_h$  cavities, there is a direct correlation between the extent of lattice expansion in  $A_3C_{60}$  and the size of the cations situated

in the  $T_d$  sites. Increased amounts of smaller ions in the  $T_d$  sites lead to lattice contraction, increased W, and a reduction in the U/W ratio, where U represents the on-site Coulomb repulsion. Conversely, larger cations expand the lattice, reduce W, and increase U/W, favoring the insulating state (Zadik et al., 2015). As the  $T_d$  sites play a more significant role than the  $O_h$  sites in determining lattice expansion in  $A_3C_{60}$  the size of the cations in these cavities is critical for tuning the electronic and structural properties of the fullerides.

The successful synthesis of fcc  $A_xCs_{3-x}C_{60}$  (A = Rb (Zadik et al., 2015) and K (Okur et al., 2024)) superconducting fullerides via a solid-state synthetic protocol involving a solid-vapor reaction has been previously reported. This process substitutes Rb and/or K\* for Cs\* in fcc  $Cs_3C_{60}$ , inducing chemical pressure that mimics the effects of physical pressurization to drive the transition from the MJTI state to a metallic/superconducting state. The goal of such chemical substitutions is to replicate the electronic response of  $Cs_3C_{60}$  under physical pressure. Achieving this requires the synthesis of materials with a high fcc phase fraction and lattice parameters that closely resemble those of the parent fcc  $Cs_3C_{60}$ .

Zadik et al. successfully synthesized a broad compositional range of fcc-rich  $Rb_xCs_{3-x}C_{60}$  (0.35  $\le$  x  $\le$  2) bulk superconducting materials (Zadik et al., 2015). However, extending this success to fcc-rich  $K_xCs_{3-x}C_{60}$  materials is significantly more challenging. This difficulty arises from the greater cation size mismatch introduced by  $K^*$  in the  $T_d$  sites, leading to increased structural disorder and elastic strain. The chemical pressure resulting from this size mismatch not only alters the bandwidth, W, but also generates static local structural disorder that gives rise to elastic strain fluctuations. These dynamical fluctuations of elastic strain in strongly correlated systems are known to profoundly affect electronic transitions, including superconductivity. In fcc  $K_xCs_{3-x}C_{60}$ , these fluctuations stem systematically from the size difference between  $K^*$  and  $Cs^*$  co-dopants (Okur et al., 2024).

Indeed, as demonstrated by Okur et al. (Okur et al., 2024), the elastic strain induced by cation compositional disorder causes a measurable attenuation of  $T_{\rm c}$ , reducing the maximum  $T_{\rm c}$  by ~12% compared to the parent  ${\rm Cs_3C_{60}}$ , where cation disorder is absent. This reduction is attributed to the variance in cation size, which links structural disorder and enhanced critical elastic strain fluctuations to the electronic ground state. These findings underscore the interplay between chemical pressure, cation disorder, and elastic strain—both static and dynamic—in tuning the superconducting properties of fullerides. A similar phenomenon has been reported for the quaternary fulleride fcc  ${\rm K_{0.25}Rb_{0.25}Cs_{2.5}C_{60}}$ , where the size

disparity among the cations within the  $T_d$  sites induces elastic strain fluctuations (Okur & Prassides, 2019).

In this study, the fcc  $K_{0.3}Cs_{0.7}C_{60}$  ternary fulleride was synthesized via a solid-state approach. This work systematically explores alternative thermal protocols for annealing and cooling, investigating reaction conditions not previously applied to over-expanded fcc-rich K<sub>x</sub>Cs<sub>3-x</sub>C<sub>60</sub>. In the previous study (Okur et al., 2024), annealing was conducted at 430°C with cooling in ambient air, yielding specific lattice parameters and fcc-phase fractions. The present work aims to determine whether modifying these thermal protocols can lead to higher fcc-phase fractions and larger lattice parameters in expanded K<sub>x</sub>Cs<sub>3-x</sub>C<sub>60</sub> fullerides. Specifically, the effects of elevated annealing temperature (480°C) and an alternative cooling method (drop-quenching in ice/water baths) compared to standard air cooling were examined, with the goal of optimizing structural and superconducting properties.

While this study primarily focuses on optimizing thermal protocols to enhance the superconducting fcc-phase fraction in ternary fullerides, it is worth noting the broader implications of superconducting materials. Beyond their fundamental significance in condensed matter physics, superconductors have practical applications in detecting magnetic anomalies due to phenomena such as the Meissner effect. This unique property enables their integration into geoinformatics and environmental science applications, including underground resource exploration, magnetic field mapping, and even earthquake or climate-related studies. As such, advancing the synthesis and phase control of superconducting materials like fullerides contributes not only to materials research but also to the development of environmental sensing and monitoring technologies.

# **Materials and Methods**

#### **Synthetic method**

All sample handling was conducted in an argon-filled glove box to protect the highly sensitive reactants from air and moisture. For transferring samples in and out of the glove box, a Swagelok fitting with a J. Young tap was employed to maintain an inert environment. Accurate amounts of phasepure  $K_6C_{60}$ ,  $Cs_6C_{60}$ , and  $C_{60}$  powders in stoichiometric ratio were weighed, blended, and ground into a fine mixture. The  $K_6C_{60}$  and  $Cs_6C_{60}$  precursors used in this study were synthesized following the previously reported protocol in (H. E. Okur, 2016) and (Okur, 2020). Their representative XRPD data and Rietveld fits are also provided in these references, as well as in (Okur et al., 2024).

*Initial annealing:* The ground mixture of K<sub>6</sub>C<sub>60</sub>, Cs<sub>6</sub>C<sub>60</sub>, and C<sub>60</sub> was pelletized and loaded into a tantalum (Ta) cell with securely fastened screw ends. This cell was placed inside a quartz tube, evacuated for 30 minutes using a high-vacuum glass manifold, and sealed under helium (He) gas pressure of 350 mbar. The sealed sample was positioned vertically in a chamber furnace, and the following thermal protocol was applied for the initial annealing, as described in (Okur et al., 2024): starting at room temperature, the furnace temperature was raised to 200°C at 5°C/min and held for 3 hours, then increased to 300°C at the same rate and maintained for 18 hours, and finally elevated to 350°C at the same rate and sustained for 120 hours. After completing this annealing step to produce a precursor, the sample was removed from the furnace, cooled to ambient temperature, and retrieved in the glove box. The resultant product was ground using a mortar and pestle.

Further annealing and cooling protocols: The precursor of K<sub>0.3</sub>Cs<sub>0.7</sub>C<sub>60</sub> was divided into four portions, each pelletized and reannealed in Ta holders sealed in quartz tubes. Each portion underwent three annealing periods of 120 hours each, performed at either 430°C or 480°C. Intermediate grinding and repelletization were performed between annealing periods to enhance crystallinity. After the final annealing, two distinct cooling methods were applied to the samples, as summarized in Table 1: (i) drop quenching: After the final grinding and pelletization step, the samples were re-annealed for 12 hours in a vertical cylindrical furnace. To achieve rapid cooling, the samples—sealed in Ta cells within quartz tubes -were introduced into the preheated furnace at the desired temperature. After annealing, the lower layer of glass wool insulating the sample was removed, and a cryogenic flask containing an ice/water bath (maintained between -3°C and 1°C) was positioned beneath the furnace. The wire suspending the sample was cut using pliers, allowing the sample to gently drop into the bath for quenching. (ii) cooling in air: In this protocol, the samples were removed from the furnace and allowed to cool naturally in ambient air after the annealing step. The final products from each experimental run were finegrained, free-flowing black powders.

**Table 1.** Summarized experimental details of the annealing and cooling treatments along with identity of the samples.

Annealing T	Cooling	Sample ID
430°C	drop-quenched	0.3@430°C_Q
430°C	cooled in air	0.3@430°C
480°C	drop-quenched	0.3@480°C_Q
480°C	cooled in air	0.3@480°C

# Structural and magnetic characterisation

X-ray powder diffraction (XRPD) measurements were conducted using a Bruker D8 ADVANCE X-ray diffractometer with DAVINCI design, utilizing Debye-Scherrer geometry and a copper source (CuK $_{\alpha}$ 1,  $\lambda$  = 1.5406 Å) over a 20 angular range spanning from 5 to 50 degrees. The polycrystalline samples were carefully loaded into glass capillaries with a diameter of 0.5 mm, sealed in an argon atmosphere. XRPD data were analyzed using the Rietveld refinement technique within the GSAS suite of Rietveld program (Larson & Von Dreele, 2004). A complex peak shape function known as pseudo-Voigt, which combines Gaussian and Lorentzian functions, was utilized to characterize peak shapes. A Chebyshev polynomial function was applied to model the background.

Magnetic properties of  $K_{0.3}C_{50.7}C_{60}$  were studied using a Quantum Design Superconducting Quantum Interference Device (SQUID) Magnetic Property Measurement System (MPMS XL) under ambient pressure conditions. The sample placed inside thin-walled 5 mm-diameter Suprasil® quartz ampoules, specially designed for SQUID measurements of airsensitive materials. To create a controlled environment, the ampoule was evacuated to approximately  $1\times10^{-4}$  mbar with the assistance of a glass high-vacuum manifold setup, for a duration of 20 minutes. Subsequently, a small amount of helium gas (typically around ~400 mbar) was introduced into the system before sealing it. The shielding fraction (SF) of sample was calculated from the ZFC magnetisation data using the following expression:

$$SF = \frac{4\pi\rho\Delta\mu}{Hm} \times 100\% \tag{1}$$

where  $\rho$  is the density of the sample (g cm<sup>-3</sup>), H is the applied external field (Oe), m is the mass of the measured sample (g) and  $\Delta\mu$  is the change in the longitudinal moment from the paramagnetic to the superconducting state.

### **Results and Discussion**

# Structural characterization

Rietveld fit of the XRPD data of  $K_{0.3}Cs_{0.7}C_{60}$  fulleride is presented in Figure 1. Rietveld analysis confirms that the compound contains additional impurity phases in addition to the  $K_{0.3}Cs_{0.7}C_{60}$  with fcc symmetry in agreement with the previous study (Okur et al., 2024). To model the data, three crystallographic phases were included in the refinement: a face-centered-cubic (fcc), body-centered orthorhombic (bco)  $\mathrm{Cs_4C_{60}}$  and  $\mathrm{CsC_{60}}$  phases. The space group  $\mathit{Fm}\overline{3}\mathit{m}$ , representing a merohedrally disordered fcc model, was employed in conjunction with a model that accounts for cation disorder to describe the fcc phase. In this model, the  $O_h$ , cavity with a radius of 2.06 Å, is significantly larger than the  $T_d$  cavity, which has a radius of 1.12 Å. Consequently, larger Cs<sup>+</sup> ions tend to accommodate in the  $O_h$  cavity, leading to its complete filling with Cs<sup>+</sup> ions. In contrast, the smaller K<sup>+</sup> ions ( $r_{K}$ <sup>+</sup> = 1.38 Å) tend to occupy the  $T_d$  cavity. As a result, the  $T_d$  cavity becomes populated by a disordered mixture of K<sup>+</sup> and Cs<sup>+</sup> ions. The validity of this approach has been confirmed through 133Cs, <sup>39</sup>K and <sup>87</sup>Rb NMR measurements (Okur et al., 2024; Zadik et al., 2015). The Cs<sub>4</sub>C<sub>60</sub> phase was modelled as the body-centeredorthorhombic (bco) (space group *Immm*) (Dahlke et al., 1998), while the CsC<sub>60</sub> phase was modelled as the orthorhombic Pmmn (Lappas et al., 1995).

The fractional atomic positions for the fcc phase were maintained at the same values as in fcc Rb<sub>3</sub>C<sub>60</sub>, where C<sub>60</sub> C-C bond distances were 1.42 Å (Zhou & Cox, 1992). However, these positions were adjusted proportionally to match the refined lattice parameters as they changed. In the fcc phase, The  $U_{\rm iso}$  values for the three distinct carbon (C) atoms, as well as for the K\* and Cs\* ions residing in the tetrahedral site, were constrained to be equal to each other, and fixed to values obtained during intermediate refinements. The K\* and Cs\* occupancy in the  $T_{\rm d}$  site of the fcc structure was held constant at their nominal values due to the insufficient quality of the data. A reliable refinement of the K\*/Cs\* occupancy of the  $T_{\rm d}$  sites as well as the  $U_{\rm iso}$  requires high-resolution

**Table 2.** Refined structural parameters for fcc-structured  $K_{0.3}Cs_{2.7}C_{60}$  (0.3@480°C\_Q) from Rietveld analysis of XRPD data collected at room temperature, with  $\lambda$  = 1.5406 Å. Column M lists the site multiplicities. The refined lattice constant is 14.6347(4) Å

x = 0.3	x/a	y/b	z/c	М	N	U <sub>iso</sub> (10 <sup>2</sup> Å <sup>2</sup> )
K	0.25	0.25	0.25	8	0.15	2.1
Cs(1)	0.25	0.25	0.25	8	0.85	2.1
Cs(2)	0.5	0.5	0.5	4	1.0	8.8
C(1)	0	0.048650	0.235947	96	0.5	0.5
C(2)	0.205948	0.078649	0.097102	192	0.5	0.5
C(3)	0.175751	0.157199	0.048650	192	0.5	0.5

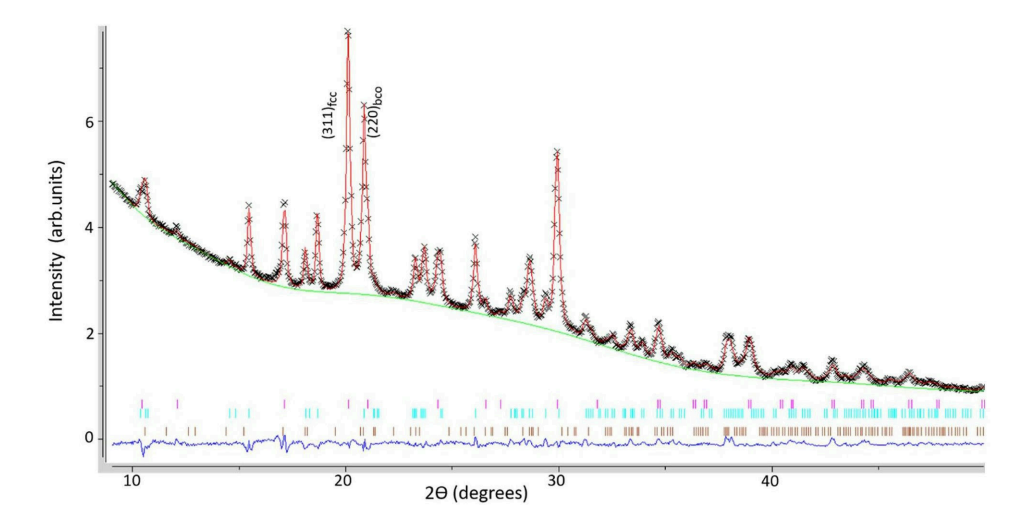


Figure 1. Rietveld fit of XRPD data for  $K_{0.3}Cs_{2.7}C_{60}$  annealed at 480°C and quenched into a cryogenic bath (0.3@480°C\_Q). Black crosses represent observed data, while red, blue, and green lines show calculated, difference, and background profiles, respectively. Ticks mark reflection positions for co-existing phases: fcc (pink), body-centered orthorhombic (bco  $Cs_4C_{60}$ , cyan), and  $CsC_{60}$  (brown) with phase fractions of 55.5(1)%, 40.4(1)%, and 4.1(3)%. The refined fcc lattice constant is 14.6347(4) Å. The most intense Bragg peaks are labeled with their (hkl) Miller indices.

synchrotron XRPD (SXRPD) data for a reliable confirmation of the stoichiometry of the compunds and thermal displacement parameters of the atoms. The fcc phase structural parameters obtained from the refinements are summarised in Table 2.

Investigations into the influence of both annealing temperature and the drop-quenching cooling technique were conducted for the  $K_{0.3}Cs_{2.7}C_{60}$  compound. Figure 2 illustrates the progression of XRPD profiles for these samples. Among them, the batch annealed at 480 °C exhibits the highest fcc-phase fraction, refining to 57.1(1)%, along with an fcc lattice parameter of 14.6204(8) Å. This aligns closely with the values obtained from the drop-quenched batch (fcc-phase fraction: 55.5(1)%, a = 14.6347(4) Å), indicating that the distinctions between quench cooling and natural air cooling are negligible.

The refined lattice parameters (a = 14.6204(8) Å for cooling in air and a = 14.6347(4) Å for drop-quenching) of  $K_{0.3}Cs_{2.7}C_{60}$  are lower than that of the disorder-free fcc  $Cs_3C_{60}$  (a = 14.76151(8) Å). This result is consistent with reduced chemical pressure due to the higher potassium content in the the  $T_d$  sites as  $K^+$  has a smaller ionic radius compared to  $Cs^+$ . For comparison, the fcc lattice parameter of nominal  $K_{0.35}Cs_{2.65}C_{60}$  annealed at 430 °C using the same synthetic protocol reported in (Okur et al., 2024) was refined to a = 14.6262(5) Å based on high-resolution synchrotron XRPD data, with phase fractions of 54.0(2)% fcc, 29.9(2)%  $Cs_4C_{60}$  and 16.1(3)%  $CsC_{60}$ .

In this study, significant fractions of competing phases are also observed, refining to 40.4(1)% Cs<sub>4</sub>C<sub>60</sub> and 4.1(3)% CsC<sub>60</sub>. It should be noted that discrepancies between refined values may arise due to the limited resolution of laboratory XRPD data compared to high-resolution synchrotron XRPD. Thus, it is not ideal to make definitive comparisons between the

refined lattice parameters and phase fractions. However, the results of this study suggest that increasing the annealing temperature positively impacts both the lattice constant and the fcc-phase fraction. These observations regarding impurity phases in  $K_xCs_{3-x}C_{60}$  compounds [22] reveal that increased  $Cs^*$  content—due to the larger size of the  $Cs^*$  ion relative to the  $T_d$  sites—drives disproportionation reactions, resulting in the co-existence of  $Cs_4C_{60}$  and  $CsC_{60}$  at the expense of the fcc-structured phases.

This phenomenon was similarly observed in the fcc  $Cs_3C_{60}$  (Ganin et al., 2010) and expanded fcc  $Rb_xCs_{3-x}C_{60}$  (Zadik et al., 2015) systems also, where the size mismatch between

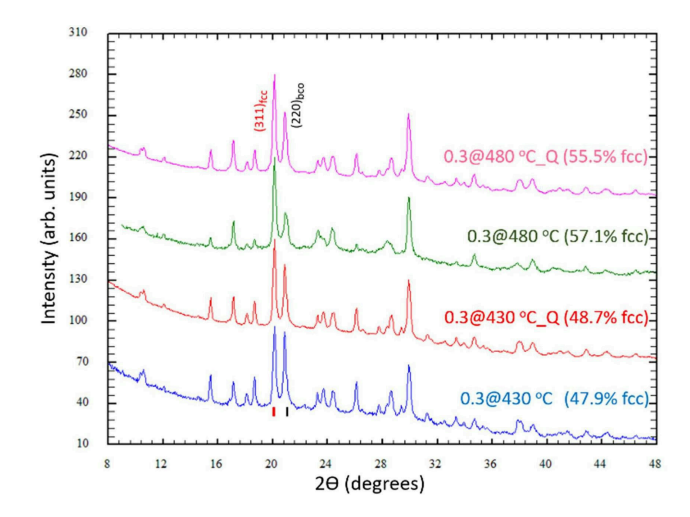


**Figure 2.** Laboratory X-ray powder diffraction profiles ( $\lambda$  = 1.5406 Å, scan speed 0.05°/min) of  $K_{0.3}Cs_{2.7}C_{60}$  samples annealed at 430 or 480 °C, cooled either in ambient air or drop quenched (Q). Red and black ticks denote the reflection positions of the (311) and (220) Bragg reflections for the face-centered cubic (fcc) and body-centered orthorhombic (bco  $Cs_4C_{60}$ ) phases, respectively.

the large Cs $^{\circ}$  and Rb $^{\circ}$  ions and the small  $T_d$  sites favors the formation of thermodynamically more stable phases such as Cs $_4$ C $_{60}$  and CsC $_{60}$ . Current results further underscore the importance of optimizing thermal protocols, particularly annealing temperatures, to enhance fcc-phase fractions while minimizing the formation of these competing impurity phases. Here, the replacement of the smaller K $^{\circ}$  ions for the Cs $^{\circ}$  cations in Cs $_3$ C $_{60}$  leads to a reduction in lattice size. This elevated potassium content in K $_{0.3}$ Cs $_{2.7}$ C $_{60}$  generates increased chemical pressure, resulting in a decreased lattice parameter of a = 14.6204(8) Å compared to Cs $_3$ C $_{60}$ . Based on the available XRPD data, it can be suggested that the increase in temperature from 430 to 480 $^{\circ}$ C has a positive impact on both the fcc lattice parameter and the fcc phase fraction.

It is important to note that these findings were derived from Rietveld refinement of laboratory XRPD data, which inherently have limited resolution. For a more comprehensive structural analysis, high-resolution SXRPD data would be required. Consequently, a direct comparison of the lattice parameters with those reported in (Okur et al., 2024) could not be performed here, as SXRPD was used for the structural analysis in that study.

# Magnetic characterization at ambient temperature

The superconducting property of  $0.3@480^{\circ}C_Q$  was explored through low-field (10 Oe) magnetization measurements across a temperature range spanning from 1.8 to 35 K, employing both the zero-field-cooled (ZFC) and field-cooled (FC) procedures. The ZFC curve demonstrates the phenomenon of flux exclusion, whereas the FC curve illustrates flux expulsion. Consequently, the temperature at which the ZFC ad FC curves diverge can be designated as the onset critical temperature ( $T_c$ ) for the superconducting material. This hysteresis in the diamagnetic susceptibility below  $T_c$ , commonly known as the Meissner effect, serves as conclusive evidence of superconductivity.

The temperature-dependent magnetization M(T) of  $K_{0.3}Cs_{2.7}C_{60}$  is shown in Figure 3. Superconductivity is observed with a  $T_{\rm c}$  of 29.9 K, as indicated by the divergence of the ZFC and FC curves. The shielding fraction, calculated from the ZFC data using Equation 1, is estimated at 18%. The refined fcc lattice

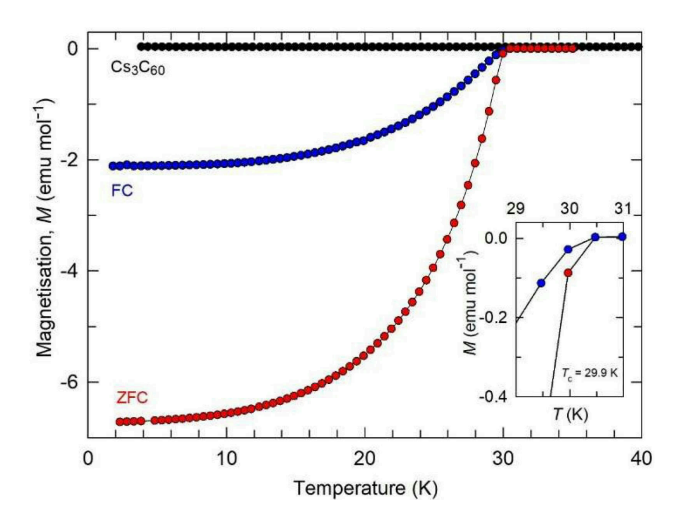


**Figure 3.** Temperature dependence of the magnetisation, M, under both zero field cooled (ZFC) and field cooled (FC) protocols, divided by the applied magnetic field (10 Oe) for  $K_{0.3}Cs_{2.7}C_{60}$  annealed at 480 °C and followed by quench cooling(0.3@480°C\_Q). Inset shows expanded region of the respective M(T) data near the superconducting  $T_c$  of 29.9 K. M(T) data for  $Cs_3C_{60}$  is sourced from (Ganin et al., 2008). Lines through data points are guides to the eye.

parameter of the compound is 14.6347(4) Å, corresponding to a  $T_c$  of 29.9 K, placing it in the over-expanded region of the electronic phase diagram of superconducting fullerides. For comparison, the nominal  $K_{0.35}Cs_{2.65}C_{60}$  (a = 14.6262(5) Å) compound reported in (Okur et al., 2024), with a = 14.6262(5) Å, exhibits a  $T_c$  of 30.4 K and a shielding fraction of 13%. These values are consistent with expectations following the global electronic phase diagram of fullerides.

#### Conclusion

The successful synthesis of  $K_{0.3}Cs_{2.7}C_{60}$  ternary fullerides highlights the critical role of thermal protocols in optimizing the structural and electronic properties of these materials. This study revisits the annealing and cooling conditions reported in (Okur et al., 2024), aiming to achieve higher fcc-phase fractions and larger lattice constants in  $K_xCs_{3-x}C_{60}$  fullerides by modifying the thermal parameters. The results show that increasing the annealing temperature from 430°C to 480°C improves the fcc-phase fraction and promotes lattice expansion. Specifically, the fcc-phase fractions increase from 48.7(1) % at 430°C to 57.1(1) % at 480°C, with a corresponding increase in lattice parameter from 14.6127(4) Å to 14.6347(4)

**Table 3.** presents the extracted values from the structural and magnetic measurements. Magnetization data for insulating fcc Cs<sub>3</sub>C<sub>60</sub> collected under a pressure of 2.6 kbar (Ganin et al., 2008) is also depicted in Figure 3, showing how substitution-induced volume contraction induces a transition from an insulating state to a metallic and subsequently superconducting state as temperature decreases.

Sample ID	a (Å)	fcc phase (wt.%)	T <sub>c</sub> (K)	SF (%)
0.3@430°C_Q	14.6127(4)	48.7(1)	n/a	n/a
0.3@480°C	14.6204(8)	57.1(1)	n/a	n/a
0.3@480°C_Q	14.6347(4)	55.5(1)	29.9	18



Å. This indicates that elevated annealing temperatures can mitigate the challenges associated with the larger size mismatch of K<sup>+</sup> and Cs<sup>+</sup> ions, which introduce structural disorder and elastic strain fluctuations.

Interestingly, the comparison between cooling methods drop-quenching and natural cooling in ambient air—reveals minimal differences in structural outcomes. This suggests that the primary factor influencing fcc-phase fractions and lattice expansion is the annealing temperature rather than the cooling protocol. However, the slight enhancement in phase fractions observed with drop-quenching may warrant further investigation, particularly at compositions closer to the Mott boundary. Magnetization measurements confirm the superconducting nature of the  $K_{0.3}Cs_{2.7}C_{60}$  with a  $T_c$  of 29.9 K observed for the batch annealed at 480°C and quenched into a cryogenic bath. This  $T_c$  is consistent with values reported for similar fullerides near the Mott boundary and reflects the interplay between lattice expansion, W, and the U/W ratio in determining superconducting behavior.

Despite these advances, several limitations remain. First, the structural analysis relies on laboratory XRPD data, which has limited resolution compared to synchrotronbased techniques. High resolution SXRPD would provide more precise insights into lattice distortions and strain fluctuations. Second, the effects of annealing temperature and cooling methods on other compositions (x) within the K<sub>x</sub>Cs<sub>3-x</sub>C<sub>60</sub> series remain unexplored and could provide a broader understanding of the phase diagram. In conclusion, optimizing annealing temperatures to 480°C enhances the fcc-phase fraction and lattice expansion in  $K_xCs_{3-x}C_{60}$ fullerides, particularly for compositions with significant cation size mismatch. While cooling methods have minimal impact on structural outcomes, the slight improvement in fcc-phase fractions with drop-quenching suggests avenues for further exploration.



Peer Review Externally peer reviewed.

Conflict of Interest The author has no conflict of interest to declare.

Financial Disclosure The author declared that this study has received no financial support.

Acknowledgments The author sincerely thanks K. Prassides for providing access to laboratory facilities and equipment essential for conducting the experiments.

#### **Author Details**

- <sup>1</sup> Bursa Technical University, Faculty of Engineering and Natural Sciences, Department of Chemistry, Bursa, Türkiye
- 0000-0003-3439-0716 ⊠ esma.okur@btu.edu.tr

#### REFERENCES

- Alloul, H., Wzietek, P., Mito, T., Pontiroli, D., Aramini, M., Riccò, M., Itie, J. P., & Elkaim, E. (2017). Mott Transition in the A15 Phase of Cs<sub>3</sub>C<sub>60</sub>: Absence of a Pseudogap and Charge Order. Physical Review Letters, 118(23), 237601.
- Dahlke, P., Henry, P. F., & Roscseinsky, M. J. (1998). Cs<sub>4</sub>C<sub>60</sub>: single phase synthesis and orientational order. Journal of Materials Chemistry, 8, 1571-1576.
- Ganin, A. Y., Takabayashi, Y., Jeglič, P., Arčon, D., Potočnik, A., Baker, P. J., Ohishi, Y., McDonald, M. T., Tzirakis, M. D., McLennan, A., Darling, G. R., Takata, M., Rosseinsky, M. J., & Prassides, K. (2010). Polymorphism control of superconductivity and magnetism in  $Cs_3C_{60}$  close to the Mott transition. Nature, 466, 221–227.
- Ganin, A. Y., Takabayashi, Y., Khimyak, Y. Z., Margadonna, S., Tamai, A., Rosseinsky, M. J., & Prassides, K. (2008). Bulk superconductivity at 38 K in a molecular system, Nat. Mater., 7, 367-371,
- Okur, H.E. (2016). Experimental Investigations of Correlated Electron Systems: Alkali Fullerides and Sesquioxides (PhD Thesis). Durham University. Durham, UK
- Ihara, Y., Alloul, H., Wzietek, P., Pontiroli, D., Mazzani, M., & Ricco, M. (2010). NMR Study of the Mott Transitions to Superconductivity in the Two  ${\rm Cs_3C_{60}}$  Phases. Physical Review Letters, 104, 256402.
- Ihara, Y., Alloul, H., Wzietek, P., Pontiroli, D., Mazzani, M., & Riccò, M. (2011). Spin dynamics at the Mott transition and in the metallic state of the Cs<sub>3</sub>C<sub>60</sub> superconducting phases. Europhysics Letters, 94(3).
- Kasahara, Y., Takeuchi, Y., Itou, T., Zadik, R. H., Takabayashi, Y., Ganin, A. Y., Arčon, D., Rosseinsky, M. J., Prassides, K., & Iwasa, Y. (2014). Spin frustration and magnetic ordering in the S = 1/2 molecular antiferromagnet fcc - Cs<sub>3</sub>C<sub>60</sub>. Phys. Rev. B, 90,
- Kasahara, Y., Takeuchi, Y., Zadik, R. H., Takabayashi, Y., Colman, R. H., McDonald, R. D., Rosseinsky, M. J., Prassides, K., & Iwasa, Y. (2017). Upper critical field reaches 90 tesla near the Mott transition in fulleride superconductors. Nature Communications,
- Klupp, G., Matus, P., Kamarás, K., Ganin, A. Y., McLennan, A., Rosseinsky, M. J., Takabayashi, Y., McDonald, M. T., & Prassides, K. (2012), Dynamic Jahn-Teller effect in the parent insulating state of the molecular superconductor Cs<sub>3</sub>C<sub>60</sub>. Nature Communications, 3(912).
- Lappas, A., Kosaka, M., Tanigaki, K., & Prassides, K. (1995). An orientationally -ordered primitive-cubic form of the fulleride CsC<sub>60</sub>. Journal of the American Chemical Society, 117, 7560–7561.
- Larson, A. C., & Von Dreele, R. (2004). General Structure Analysis System (GSAS). Los Alamos National Laboratory Report LAUR, 86-748.
- Lee, P. A., Nagaosa, N., & Wen, X.-G. (2006). Doping a Mott insulator: Physics of hightemperature superconductivity. Reviews of Modern Physics, 78(1), 17–85.
- Menelaou, M., Takabayashi, Y., Okur, H. E., Zadik, R. H., & Prassides, K. (2018). Structural and electronic response of overexpanded superconducting fullerides close to the Mott insulator boundary. International Journal of Modern Physics B, 1840020.
- Nomura, Y., Sakai, S., Capone, M., & Arita, R. (2015). Unified understanding of superconductivity and Mott transition in alkali-doped fullerides from first principles. Science Advances, 1(7), e1500568-e1500568.
- Okur, H. E. (2020). Synthesis and structural analysis of non-stoichiometric ternary  $fulleride \ K_{1.5}Ba_{0.25}CsC_{60}. \ \textit{Turk J Chem}.$
- Okur, H. E., Colman, R. H., Takabayashi, Y., Jeglič, P., Ohishi, Y., Kato, K., Arčon, D., Kubota, Y., & Prassides, K. (2024). Fulleride superconductivity tuned by elastic strain due to cation compositional disorder. Chem. Sci., 15(40), 16485–16493.
- Okur, H. E., & Prassides, K. (2019). Structural and electronic properties of the overexpanded quaternary superconducting fulleride  $K_{0.25}Rb_{0.25}Cs_{2.5}C_{60}$ . Journal of Physics and Chemistry of Solids, 131, 44-49.
- Potocnik, A., Ganin, A. Y., Takabayashi, Y., McDonald, M. T., Heinmaa, I., Jeglic, P., Stern, R., Rosseinsky, M. J., Prassides, K., & Arcon, D. (2014). Jahn-Teller orbital glass state in the expanded fcc  $Cs_3C_{60}$  fulleride. Chemical Science, 5, 3008–3017.
- Potočnik, A., Krajnc, A., Jeglič, P., Takabayashi, Y., Ganin, A. Y., Prassides, K., Rosseinsky, M. J., & Arčon, D. (2014). Size and symmetry of the superconducting gap in the f.c.c.  $\mathrm{Cs_3C_{60}}$  polymorph close to the metal-Mott insulator boundary. Scientific Reports,

- Si, Q., & Steglich, F. (2010). Heavy fermions and quantum phase transitions. Science (New York, N.Y.), 329(5996), 1161–1166.
- Takabayashi, Y., Ganin, A. Y., Jeglic, P., Arcon, D., Takano, T., Iwasa, Y., Ohishi, Y., Takata, M., Takeshita, N., Prassides, K., & Rosseinsky, M. J. (2009). The disorder-free non-BCS superconductor Cs<sub>3</sub>C<sub>60</sub> emerges from an antiferromagnetic insulator parent state. *Science*, 323(5921), 1585–1590.
- Takabayashi, Y., & Prassides, K. (2016a). The Renaissance of Fullerene Superconductivity. In D. Mingos (Ed.), 50 years of structure and bonding - The anniversary volume (pp. 119–138). Springer US.
- Takabayashi, Y., & Prassides, K. (2016b). Unconventional high-Tc superconductivity in fullerides. *Philosophical Transactions of the Royal Society A*, 374(2076).
- Uemura, Y. J. (2009). Commonalities in phase and mode. *Nature Materials*, 8(4), 253–255.
- Wzietek, P., Mito, T., Alloul, H., Pontiroli, D., Aramini, M., & Ricco, M. (2014). NMR Study of the Superconducting Gap Variation near the Mott Transition in Cs<sub>3</sub>C<sub>60</sub>. *Physical Review Letters*, 112, 5.
- Zadik, R. H., Takabayashi, Y., Colman, R. H., Garbarino, G., & Prassides, K. (2018).Pressure-induced Mott-insulator-metal crossover at ambient temperature in an overexpanded fulleride. *Materials Chemistry Frontiers*, 2(5), 993–998.
- Zadik, R. H., Takabayashi, Y., Klupp, G., Colman, R. H., Ganin, A. Y., Potocnik, A., Jeglic, P., Arcon, D., Matus, P., Kamaras, K., Kasahara, Y., Iwasa, Y., Fitch, A. N., Ohishi, Y., Garbarino, G., Kato, K., Rosseinsky, M. J., & Prassides, K. (2015). Optimized unconventional superconductivity in a molecular Jahn-Teller metal. Science Advances, 1, e1500059.
- Zhou, O., & Cox, D. E. (1992). Structures of C<sub>60</sub> intercalation compounds. *Journal of Physics and Chemistry of Solids*, 53(11), 1373–1390.